

This is the **accepted version** of the article:

García-Sobrino, Joaquín; Pinho, Armando J.; Serra Sagristà, Joan. «Competitive Segmentation Performance on Near-lossless and Lossy Compressed Remote Sensing Images». IEEE geoscience and remote sensing letters, (August 2019). DOI 10.1109/LGRS.2019.2934997

This version is available at <https://ddd.uab.cat/record/215774>

under the terms of the  **CC BY** COPYRIGHT license

Competitive Segmentation Performance on Near-lossless and Lossy Compressed Remote Sensing Images

Joaquín García-Sobrino, Armando J. Pinho, *Member, IEEE*, and Joan Serra-Sagrístà, *Senior Member, IEEE*

Abstract—Image segmentation lies at the heart of multiple image processing chains, and achieving accurate segmentation is of utmost importance as it impacts later processing. Image segmentation has recently gained interest in the field of remote sensing, mostly due to the widespread availability of remote sensing data. This increased availability poses the problem of transmitting and storing large volumes of data. Compression is a common strategy to alleviate this problem. However, lossy or near-lossless compression prevents a perfect reconstruction of the recovered data. This letter investigates the image segmentation performance in data reconstructed after a near-lossless or a lossy compression. Two image segmentation algorithms and two compression standards are evaluated on data from several instruments. Experimental results reveal that segmentation performance over previously near-lossless and lossy compressed images is not markedly reduced at low and moderate compression ratios. In some scenarios, accurate segmentation performance can be achieved even for high compression ratios.

Index Terms—Remote sensing data, image segmentation, lossy compression, near-lossless compression, maximum likelihood, successive band merging, JPEG 2000, JPEG-LS.

I. INTRODUCTION

IMAGE segmentation is generally defined as the process of partitioning an image into regions (or segments). The underlying idea consists of dividing an image into homogeneous segments by grouping neighbouring pixels that follow a similarity criteria. The main purpose is to estimate the structure of the scene and to extract image objects and boundaries for subsequent object-based analysis.

In the field of remote sensing, image segmentation is an essential step of low-level image analysis and is usually performed in the first stages of a processing chain [1]. Efficiently segmented images are required in a wide variety of applications, such as object detection [2], land cover classification [3], or landscape change detection [4].

Advances in remote sensing technology have led to improve the quality of the harvested data in terms of spectral and spatial resolution, and allowed to reveal more ground details. Segmentation results have thus been improved due

to the rich information contained in the images. Several of the existing segmentation algorithms rely on two main traditional strategies: 1) region-based methods, which depend on region information, and 2) edge-based methods, which look for boundaries between objects to find them [5], [6]. Both strategies have proven to achieve competitive segmentation results.

However, improving the quality of the acquired data has also led to increase the size of the collected data, requiring more means for transmission and storage. Data compression is an effective way to reduce the volume of the collected data. Nonetheless, achieving high compression ratios usually entails some level of distortion in the recovered scene, which may compromise the usefulness of the reconstructed data and prevent achieving good segmentation results. Texture blurring and unclear edges between objects can be a consequence of near-lossless and lossy compression. These effects can make image segmentation a major challenge, because of difficulties in detecting homogeneous regions or boundaries [7].

The impact of a near-lossless or lossy compression stage on subsequent processes is lately receiving a lot of attention: in the scope of classification applications, different strategies to perform classification on previously compressed images were presented in [8]–[11]. Results revealed that the classification accuracy was still reliable after the compression stage, even at high compression ratios. Similar conclusions were yielded for anomaly detection [12], [13] for linear spectral unmixing [14], [15], and for statistical retrieval algorithms [16]–[18]. To the best of our knowledge, a similar study on the impact of compression on image segmentation has not been presented.

The aim of this work is to investigate the performance of image segmentation in remote sensing images reconstructed after a near-lossless or a lossy compression. This analysis, carried out in an early stage of the processing chain, can determine the usefulness of the data for subsequent processing (classification, detection, ...). Segmentations on the reconstructed scenes are evaluated with respect to segmentations on the original scenes to determine the impact of compression.

For near-lossless compression, we employ the JPEG-LS standard [19], which has been widely used in compression of high-resolution remote sensing data due to the speed and efficiency provided. For lossy compression, the JPEG 2000 standard [20] is employed, because it supplies a set of features that are important in the field of remote sensing, such as competitive low bit-rate performance, progressive quality image transmission, random codestream access, etc. These features make both JPEG-LS and JPEG 2000 standards highly attractive in the context of remote sensing applications.

For the segmentation stage, two segmentation algorithms are

Manuscript received August 10, 2019.

JGS and JSS are with the Group on Interactive Coding of Images, Universitat Autònoma de Barcelona, Spain. Web: <http://www.gici.uab.cat>. E-mail: joaquin.garcia.sobrino@deic.uab.cat; Joan.Serra@uab.cat.

AJP is with the Informatics Systems and Processing Group (ISP), Institute of Electronics and Informatics Engineering of Aveiro (IEETA), Universidade de Aveiro, Aveiro, Portugal. Web: <http://www.ieeta.pt>. E-mail: ap@ua.pt.

This work was supported in part by the Spanish Ministry of Economy and Competitiveness and by the European Regional Development Fund under Grant RTI2018-095287-B-I00, by the Catalan Government under Grant 2017SGR-463, by Portuguese Funds through the FCT - Foundation for Science and Technology, under the project UID/CEC/00127/2013, and by the Santander Bank under Grant Program "Ibero-America Santander Research".

employed: Maximum Likelihood (ML) [21] and Successive Band Merging (SBM) [22]. ML is a simple segmentation technique, whose low computational complexity is suitable for remote sensing imagery. It has become an accepted estimate used as the baseline for more complex algorithms [23], [24]. SBM is a recent segmentation algorithm specifically designed for multispectral remote sensing images.

The remainder of the letter is organized as follows. Section II describes the compression techniques and the segmentation algorithms used in the experiments. Section III presents the data collection and the parameter setting. Section IV reports the experimental results. Conclusions are drawn in Section V.

II. METHODS

This section describes the segmentation techniques and the compression standards used in the experiments.

A. Segmentation Algorithms

For image segmentation we use two methods: an algorithm based on the well-known ML approach and a novel method based on Markov Random Fields (MRF), the SBM algorithm. Both methods have shown good performance on several remote sensing datasets [22], [25].

The ML algorithm computes the probability that a specific pixel belongs to a particular region. The algorithm assumes that the statistics for each region in the scene follow a normal distribution. Each pixel will be part of the region that has the highest probability, considering that, if the highest probability falls below a given threshold, then the pixel will not be assigned to any region. SBM is a segmentation algorithm devised to work with multispectral remote sensing images. The segmentation process is carried out through three stages. In the initial step, the maximizer of the posterior marginals (MPM) is estimated. In the second stage, contextual information is included in a nonparametric way. Finally, each pixel is assigned to a region in the scene [22].

B. Compression Standards

For image compression we consider two paradigms: near-lossless and lossy compression. On the one hand, near-lossless compression is used to control the maximum absolute error per sample introduced in the reconstructed data. On the other hand, lossy compression is employed to control the overall bit-rate. Two standard coding techniques are employed in the experiments: JPEG-LS for near-lossless compression and JPEG 2000 for lossy compression. JPEG-LS is a lossless and near-lossless compression standard that provides simplicity, low computational complexity and memory requirements. JPEG 2000 is an international standard that provides an extensive range of features in a single compressed bit-stream for a large amount of applications, such as remote sensing imagery, medical diagnostic imaging, and mobile communications, among others.

III. DATA AND EXPERIMENTAL SETTINGS

This section presents the datasets and the parameter configurations used in the experiments.

TABLE I: Characteristics of the datasets. Number of scenes per instrument and sizes are reported.

Instrument	Number of scenes	Average size (spectral channels \times rows \times columns)
AVIRIS	2	$212 \times 160 \times 160$
Landsat 8	1	$8 \times 800 \times 500$
QuickBird	20	$4 \times 1052 \times 1182$
RODIS	2	$103 \times 642 \times 416$

A. Data Collection

To conduct the experiments, 25 images from four different remote sensing instruments were studied. We selected images and ground truth data devised for the testing of segmentation algorithms. In order to study a set of representative data, the tested datasets included images with different spectral and spatial resolution, dissimilar number of spectral channels, obtained from different instruments, and scanned on distinct scenarios. The scenes were captured over rural and urban areas and contain buildings, roads, grass, trees, crops, water, and railways, among other objects. Table I provides the characteristics for the datasets. Most of the images are public and available at [26], [27].

B. Experimental Settings and Software

For near-lossless compression, the maximum absolute error per sample introduced in the data was controlled using seven Peak Absolute Errors (PAE), $\delta \in \{1, 3, 7, 15, 31, 63, 127\}$. Higher values of the PAE originate higher compression ratios, but the level of distortion introduced is also increased. For lossy compression, the overall bit-rate was controlled using six target bit-rates, distributed between 4 and 0.1 bits per pixel per component (bpppc). It is expected that providing an analysis of the signal in terms of frequency components benefits the coding. Therefore, the wavelet transform was used to provide a more decorrelated and compact representation of the signal. In the experiments, six levels of the Discrete Wavelet Transform (DWT) were applied in the spatial dimension to exploit the spatial redundancy present in the scene.

The segmentation stage was carried out on the original and on the reconstructed data. Both the ML and the SBM algorithms were evaluated on the four datasets. To start the segmentation process, the selected algorithms needed an initial segmentation. All experiments started from an initial segmentation obtained from k-means [28]. Default options were used for the remaining parameters.

To achieve a fair comparison, the parameter configuration was kept constant for all compression and segmentation experiments, in such a way that we used suitable settings for the characteristics of all the images. The software implementations employed for compression were: JPEG-LS software [29] for JPEG-LS and Kakadu software [30] for JPEG 2000. The segmentation stage (ML and SBM algorithms) was carried out using the Markov-Models toolbox [31] employed in [22].

IV. EXPERIMENTAL RESULTS

This section presents the experimental results. The proposed sequential chain includes first a compression stage. At the

TABLE II: Region and content of the scenes.

Instrument	Identifier	Region	Content
AVIRIS	Indian Pines	Rural area (Indiana)	Alfalfa, corn, grass, wheat, woods, and buildings, among others
Landsat 8	Humid Pampas	Rural area (Argentina)	Wildfire, corn, fallow land, and water, among others
QuickBird	zh11	Urban area (Zurich town)	Roads, buildings, trees, grass, water, and railways, among others
ROSIS	Pavia University	Urban area (Pavia town)	Asphalt, meadows, trees, buildings, and shadows, among others

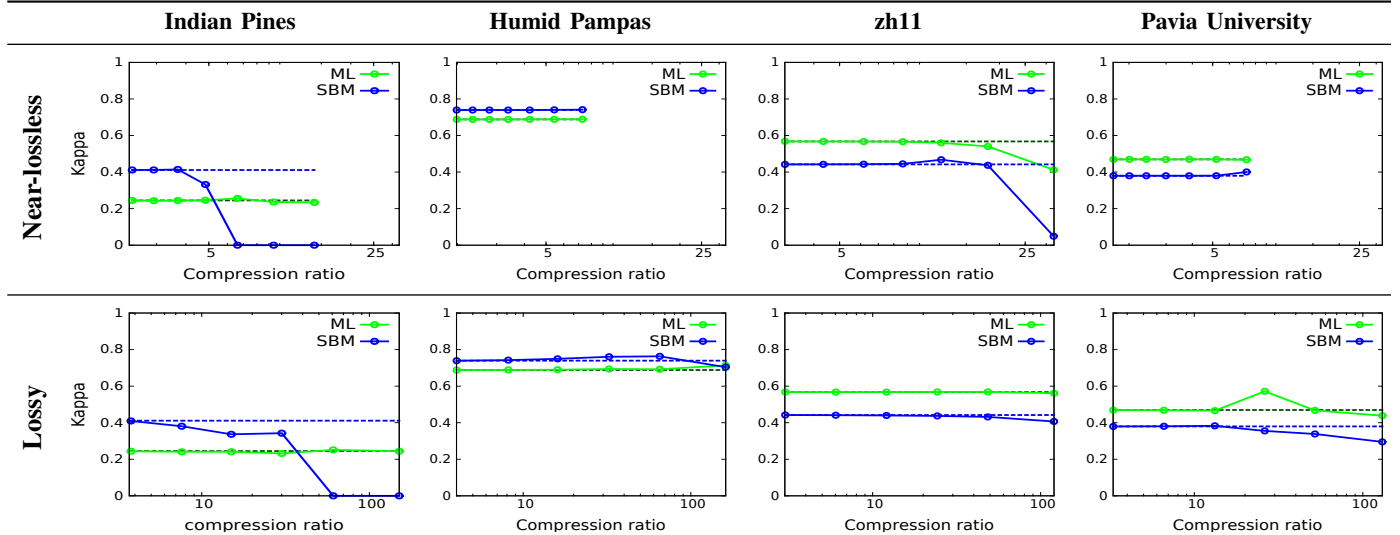


Fig. 1: Segmentation performance in $\hat{\kappa}$ (higher is better) for near-lossless (upper row) and lossy compression (lower row). In the plots, the vertical axis represents the segmentation performance ($\hat{\kappa}$) and the horizontal axis represents the compression ratio. Results using reconstructed data are plotted in solid lines and results using uncompressed data (original image) are plotted in dashed lines. Each mark represents the segmentation performance achieved when the scene has been previously compressed at a particular compression ratio. Results for the ML algorithm are plotted in green lines and results for the SBM algorithm are plotted in blue lines. Each column shows results for a particular scene.

receiver side the scene is decoded, then image segmentation is carried out on the reconstructed data.

A. Segmentation Assessment

The segmentation performance was assessed with respect to handmade ground truth segmentations. Following the strategy used in [22], we used Cohen's kappa coefficients ($\hat{\kappa}$) [32] to compare the performance of the different schemes adopted. The $\hat{\kappa}$ coefficient provides a measure of agreement between the machine segmentation and the human ground truth. Complete agreement corresponds to $\hat{\kappa} = 1$, and lack of agreement corresponds to $\hat{\kappa} = 0$.

Here, segmentation results are reported for four scenes (one from each dataset). Results for the remaining images from each dataset are similar. Table II provides characteristics for the scenes reported. Detailed experimental results for the 25 scenes described in Table I are provided as supplementary material at http://gici.uab.cat/pub/coding_segmentation/.

Figure 1 illustrates the segmentation performance for the near-lossless and lossy compression settings proposed. Plots show the $\hat{\kappa}$ coefficients for different compression ratios when the ML and SBM algorithms are used in the segmentation stage. Results using original data (uncompressed) are also provided for comparison purposes. The relationship between PAEs/target bit-rates and compression ratios and the SNR Energy achieved by each compression setting are reported in

Table III. One can see that, for near-lossless, compression ratios of about 10:1 allow to achieve at least the same segmentation performance as with the original data. Only the Indian Pines scene requires lower compression ratios of, approximately, 4:1 to keep the segmentation results unchanged when the SBM algorithm is employed. SBM uses the spectral information to obtain the most probable state of each pixel. When the compression ratio increases, too much distortion may be introduced in the spectral dimension, which is reflected in the performance of the SBM algorithm.

In a lossy scenario, compression ratios of about 25:1 allow to retain enough features to achieve the same segmentation performance as with uncompressed data. As for the case of near-lossless compression, the Indian Pines scene begins to decrease the segmentation performance at lower compression ratios of, approximately, 8:1 when the SBM algorithm is employed. It is interesting to note that the ML algorithm achieves higher $\hat{\kappa}$ coefficients compared to the SBM method when the spatial resolution of the scene is high and vice versa. While ML does not take into account relations between neighboring pixels, SBM does. If there are no relations, the performance might decrease, which is likely to occur when the spatial resolution is high.

The reported results reveal that the segmentation performance over previously near-lossless and lossy compressed scenes is not markedly reduced at low and moderate compression ratios. Nonetheless, lossy compression allows to keep the

TABLE III: For Near-lossless (Peak Absolute Error, PAE) and Lossy(target bit-rate, BR) compression, compression ratio (CR), Bpppc and SNR Energy (in dB) are reported. The dynamic range of the original image is provided in parenthesis. The corresponding experiments for the segmentation results reported in Fig.2 are here marked in italic font.

	Indian Pines (14 bpppc)			Humid Pampas (15 bpppc)			zh11 (12 bpppc)			Pavia University (13 bpppc)		
PAE	CR	bpppc	SNR	CR	bpppc	SNR	CR	bpppc	SNR	CR	bpppc	SNR
1	2.4:1	5.8	71.6	2.0:1	7.5	85.1	3.1:1	3.9	50.5	1.7:1	7.6	66.1
3	2.9:1	4.8	63.8	2.3:1	6.5	77.3	4.3:1	2.8	42.8	2.0:1	6.5	58.4
7	3.7:1	3.8	57.1	2.8:1	5.4	70.6	6.2:1	1.9	36.3	2.4:1	5.4	51.7
15	4.8:1	2.9	50.9	3.4:1	4.4	64.3	8.6:1	1.4	30.2	3.0:1	4.3	45.3
31	6.6:1	2.1	45.0	4.2:1	3.6	58.1	12.1:1	1.0	24.3	3.9:1	3.3	39.2
63	9.4:1	1.5	39.1	5.4:1	2.8	52.1	18.1:1	0.7	18.5	5.2:1	2.5	33.1
127	14.0:1	1.0	33.3	7.3:1	2.1	46.2	32.0:1	0.4	12.8	7.2:1	1.8	27.3
BR												
4	3.8:1	3.7	56.9	4.0:1	3.8	59.8	3.0:1	4.0	53.2	3.3:1	3.9	41.5
2	7.6:1	1.8	44.5	8.1:1	1.9	46.5	6.0:1	2.0	41.5	6.6:1	2.0	30.5
1	15.0:1	0.9	36.7	16.0:1	0.9	39.8	12.1:1	1.0	33.5	13.2:1	1.0	24.4
0.5	30.0:1	0.5	31.4	32.5:1	0.5	35.2	24.2:1	0.5	27.7	26.2:1	0.5	20.3
0.25	60.9:1	0.2	28.0	65.3:1	0.2	32.7	48.4:1	0.3	23.3	52.0:1	0.25	17.3
0.1	150.5:1	0.1	25.1	161.5:1	0.1	29.5	120.0:1	0.1	18.7	130.4:1	0.1	14.3

segmentation results unchanged at higher compression ratios compared to near-lossless compression. This is due to the different nature of the distortion introduced by near-lossless and lossy compression. The impact of compression is the same for both the ML and SBM algorithms. Only in the case of the Indian Pines scene, the SBM algorithm is affected more significantly by compression than the ML algorithm.

Figure 2 reports the handmade ground truth employed to assess the segmentation performance and some segmentation results for the ML and SBM algorithms. This figure shows the segmented images when the original scene and the reconstructed data from near-lossless and lossy compression are used in the segmentation stage. For reconstructed data, the higher compression ratio that allows to achieve competitive segmentation performance for both the ML and SBM algorithms is displayed.

V. CONCLUSIONS

In this letter, the performance of image segmentation on scenes that had gone through a compression and decompression stage was investigated. In the compression stage, the JPEG-LS and the JPEG 2000 standards were used to perform near-lossless and lossy compression, respectively. Image segmentation was carried out using the ML and SBM algorithms.

Experimental results revealed that low and moderate compression ratios do not reduce the performance of the segmentation algorithms when reconstructed data is used. Near-lossless compression allowed to produce the same segmentation performance as with the original data at compression ratios of, approximately, 10:1. For lossy compression, unchanged segmentations were achieved at compression ratios of, approximately, 25:1. The impact of compression was similar for both the ML and SBM algorithms and the different scenarios analyzed. Only in the case of the Indian Pines scene, segmentation results remained unchanged at compression ratios of 4:1 and 8:1 for near-lossless and lossy compression, respectively, when the SBM algorithm was used. These observations are consistent with similar results reported for other scientific areas and may benefit the development of upcoming remote sensing

instruments, image processing chains, and image analysis applications.

REFERENCES

- [1] V. Dey, Y. Zhang, and M. Zhong, "A review on image segmentation techniques with remote sensing perspective," in *ISPRS TC VII Symposium 100 Years ISPRS*, 2010, pp. 31–42.
- [2] R. G. Cinbis, J. Verbeek, and C. Schmid, "Segmentation Driven Object Detection with Fisher Vectors," in *Proc. of the IEEE International Conference on Computer Vision*, 2013, pp. 2968–2975.
- [3] L. Zhang, K. Jia, X. Li, Q. Yuan, and X. Zhao, "Multi-scale segmentation approach for object-based land-cover classification using high-resolution imagery," *Remote Sensing Letters*, vol. 5, no. 1, pp. 73–82, 2014.
- [4] L. Ma, M. Li, T. Blaschke, X. Ma, D. Tiede, L. Cheng, Z. Chen, and D. Chen, "Object-Based Change Detection in Urban Areas: The Effects of Segmentation Strategy, Scale, and Feature Space on Unsupervised Methods," *Remote Sensing*, vol. 8, no. 9, p. 761, 2016.
- [5] M. Mueller, K. Segl, and H. Kaufmann, "Edge- and region-based segmentation technique for the extraction of large, man-made objects in high-resolution satellite imagery," *Pattern Recognition*, vol. 37, no. 8, pp. 1619–1628, 2004.
- [6] H. G. Kaganami and Z. Beiji, "Region-based segmentation versus edge detection," in *IEEE International Conference on Intelligent Information Hiding and Multimedia Signal Processing (IIH-MSP'09)*, September 2009, pp. 1217–1221.
- [7] S. Deng, Y. Zhang, and S. Tian, "Building surface texture segmentation in urban remote sensing image using improved ORTSEG algorithm," in *IEEE Geoscience and Remote Sensing Symposium (IGARSS)*, July 2015, pp. 4348–4351.
- [8] I. Blanes and J. Serra-Sagrà, "Quality evaluation of progressive lossy-to-lossless remote-sensing image coding," in *16th IEEE International Conference in Image Processing (ICIP)*, 2009, pp. 3709–3712.
- [9] A. Zabala and X. Pons, "Effects of lossy compression on remote sensing image classification of forest areas," *International Journal of Applied Earth Observation and Geoinformation*, vol. 13, no. 1, pp. 43–51, 2011.
- [10] F. García-Vilchez, J. Muñoz-Marí, M. Zortea, I. Blanes, V. González-Ruiz, G. Camps-Valls, A. Plaza, and J. Serra-Sagrà, "On the impact of lossy compression on hyperspectral image classification and unmixing," *IEEE Geoscience and Remote Sensing Letters*, vol. 8, no. 2, pp. 253–257, 2011.
- [11] Z. Chen, Y. Hu, and Y. Zhang, "Effects of compression on remote sensing image classification based on fractal analysis," *IEEE Transactions on Geoscience and Remote Sensing*, vol. 57, no. 7, pp. 4577–4590, 2019.
- [12] G. Carvajal, B. Penna, and E. Magli, "Unified lossy and near-lossless hyperspectral image compression based on JPEG 2000," *IEEE Geoscience and Remote Sensing Letters*, vol. 5, no. 4, pp. 593–597, 2008.
- [13] Q. Du and J. E. Fowler, "Hyperspectral image compression using JPEG 2000 and principal component analysis," *IEEE Geoscience and Remote Sensing Letters*, vol. 4, no. 2, pp. 201–205, 2007.
- [14] Q. Du and C. I. Chang, "Linear mixture analysis-based compression for hyperspectral image analysis," *IEEE Transactions on Geoscience and Remote Sensing*, vol. 42, no. 4, pp. 875–891, 2004.

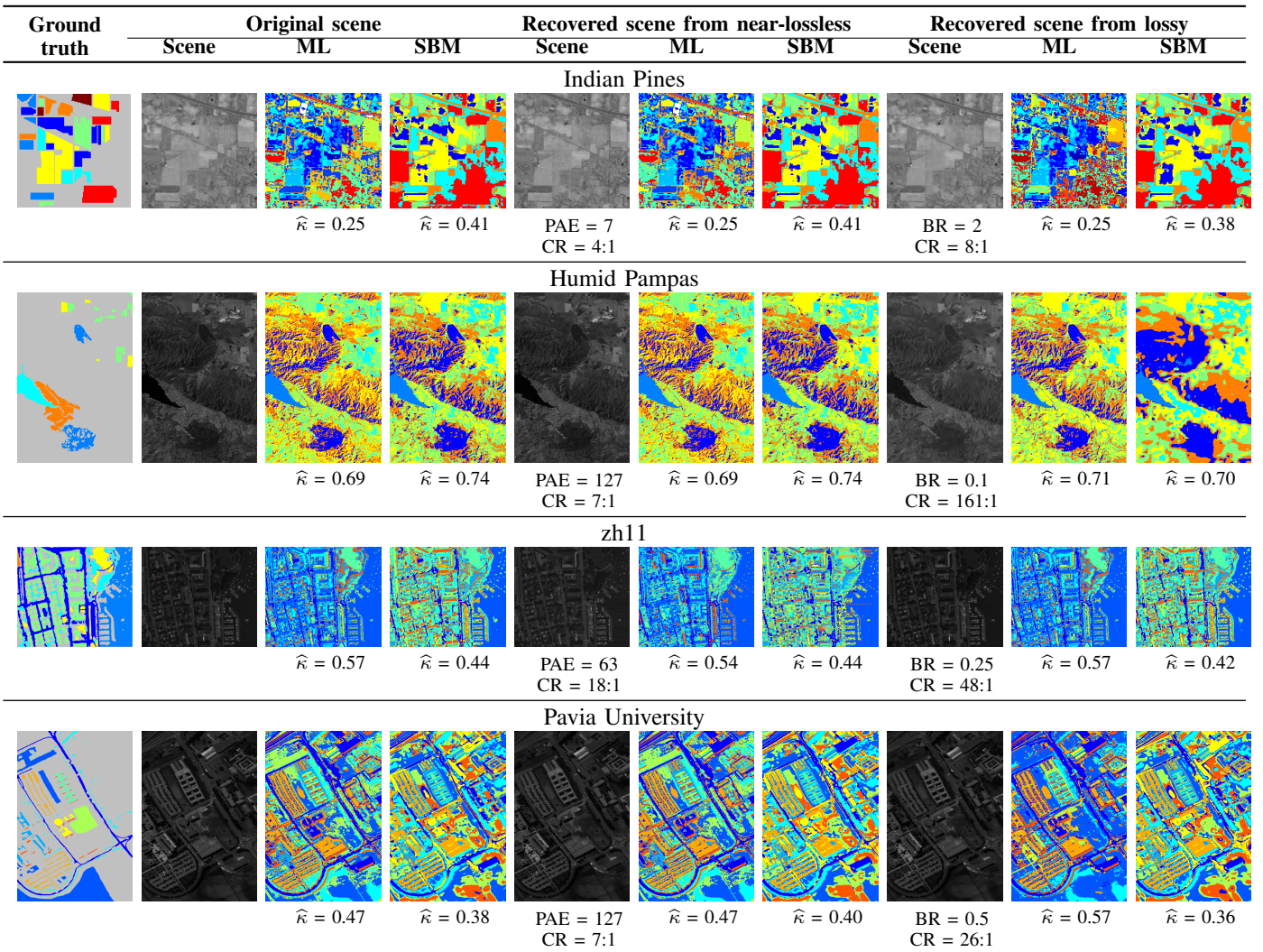


Fig. 2: Ground truth and segmentation results of the original and the reconstructed data. Each row shows a particular scene. Results are plotted for both the ML and SBM algorithms. The PAE/target bit-rate (BR) used in the compression stage and the compression ratio (CR) achieved are reported for each scene. The $\hat{\kappa}$ coefficient is reported for each segmentation.

- [15] M. Zortea and A. Plaza, "Spatial preprocessing for endmember extraction," *IEEE Transactions on Geoscience and Remote Sensing*, vol. 47, no. 8, pp. 2679–2693, 2009.
- [16] J. García-Sobrino, I. Blanes, V. Laparra, G. Camps-Valls, and J. Serra-Sagristà, "Impact of near-lossless compression of IASI LIC data on statistical retrieval of atmospheric profiles," in *Proc. of On-Board Payload Data Compression Workshop (OBPDC)*, Venice, Italy, October 2014.
- [17] J. García-Sobrino, J. Serra-Sagristà, V. Laparra, X. Calbet, and G. Camps-Valls, "Statistical atmospheric parameter retrieval largely benefits from spatial-spectral image compression," *IEEE Transactions on Geoscience and Remote Sensing*, vol. 55, no. 4, pp. 2213–2224, 2017.
- [18] J. García-Sobrino, V. Laparra, J. Serra-Sagristà, X. Calbet, and G. Camps-Valls, "Improved Statistically Based Retrievals via Spatial-Spectral Data Compression for IASI Data," *IEEE Transactions on Geoscience and Remote Sensing*, pp. 1–18, 2019.
- [19] M. J. Weinberger, G. Seroussi, and G. Sapiro, "The LOCO-I lossless image compression algorithm: Principles and standardization into JPEG-LS," *IEEE Transactions on Image Processing*, vol. 9, no. 8, pp. 1309–1324, August 2000.
- [20] D. Taubman and M. Marcellin, *JPEG 2000 image compression fundamentals, standards and practice: image compression fundamentals, standards and practice*. Springer Science & Business Media, 2012.
- [21] A. Dempster, N. M. Laird, and D. B. Rubin, "Maximum likelihood from incomplete data via the EM algorithm," *Journal of the Royal Statistical Society. Series B (methodological)*, pp. 1–38, 1977.
- [22] J. Baumgartner, J. Gimenez, M. Scavuzzo, and J. Pucheta, "A new approach to segmentation of multispectral remote sensing images based on MRF," *IEEE Geoscience and Remote Sensing Letters*, vol. 12, no. 8, pp. 1720–1724, 2015.
- [23] A. Sarti, C. Corsi, E. Mazzini, and C. Lamberti, "Maximum likelihood segmentation of ultrasound images with Rayleigh distribution," *IEEE Transactions on Ultrasonics, Ferroelectrics, and Frequency Control*, vol. 52, no. 6, pp. 947–960, 2005.
- [24] I. B. Ayed, A. Mitiche, and Z. Belhadj, "Polarimetric image segmentation via maximum-likelihood approximation and efficient multiphase level-sets," *IEEE Transactions on Pattern Analysis & Machine Intelligence*, vol. 9, pp. 1493–1500, 2006.
- [25] J. M. Beaulieu and R. Touzi, "Segmentation of textured polarimetric sar scenes by likelihood approximation," *IEEE Transactions on Geoscience and Remote Sensing*, vol. 42, no. 10, pp. 2063–2072, 2004.
- [26] GIC, "Hyperspectral remote sensing scenes," Available: http://www.ehu.eu/ccwintco/index.php?title=Hyperspectral_Remote_Sensing_Scenes.
- [27] M. Volpi and V. Ferrari, "Zurich summer dataset," Available: <https://sites.google.com/site/michelevolpiperesearch/data/zurich-dataset>.
- [28] T. Kanungo, D. M. Mount, N. S. Netanyahu, C. Piatko, R. Silverman, and A. Y. Wu, "An efficient k-means clustering algorithm: Analysis and implementation," *IEEE Transactions on Pattern Analysis & Machine Intelligence*, vol. 7, pp. 881–892, 2002.
- [29] D. A. Clunie, "JPEG-LS," <http://www.dclunie.com/jpegls.html>.
- [30] D. S. Taubman, "Kakadu software," <http://www.kakadusoftware.com/>.
- [31] J. Baumgartner, "Markov-Models toolbox for segmentation of images and local data," 2015, LIMAC, FCFEYN.
- [32] J. Cohen, "A coefficient of agreement for nominal scales," *Educational and psychological measurement*, vol. 20, no. 1, pp. 37–46, 1960.